

# Catalysis Science & Technology

Accepted Manuscript



This article can be cited before page numbers have been issued, to do this please use: R. Nasrollahi, A. Heydari-turkmani and S. Zakavi, *Catal. Sci. Technol.*, 2019, DOI: 10.1039/C8CY02433B.



This is an Accepted Manuscript, which has been through the Royal Society of Chemistry peer review process and has been accepted for publication.

Accepted Manuscripts are published online shortly after acceptance, before technical editing, formatting and proof reading. Using this free service, authors can make their results available to the community, in citable form, before we publish the edited article. We will replace this Accepted Manuscript with the edited and formatted Advance Article as soon as it is available.

You can find more information about Accepted Manuscripts in the [author guidelines](#).

Please note that technical editing may introduce minor changes to the text and/or graphics, which may alter content. The journal's standard [Terms & Conditions](#) and the ethical guidelines, outlined in our [author and reviewer resource centre](#), still apply. In no event shall the Royal Society of Chemistry be held responsible for any errors or omissions in this Accepted Manuscript or any consequences arising from the use of any information it contains.

Journal Name

## ARTICLE

## Kinetic and mechanistic aspects of solid state, nanostructured porphyrin diacid photosensitizers in photooxidation of sulfides

Rahele Nasrollahi, Akram Heydari-turkmani and Saeed Zakavi\*

Received 00th January 20xx,  
Accepted 00th January 20xx

DOI: 10.1039/x0xx00000x

www.rsc.org/

In continuing our studies on the photocatalytic performance of porphyrin diacids, kinetics and mechanism of the photooxidation of para-substituted phenyl methyl sulfides (para X = H, CH<sub>3</sub>, OCH<sub>3</sub>, Cl, F) catalyzed by a series of *meso*-tetra(aryl)porphyrins (aryl = phenyl, 2-chlorophenyl, 2-methylphenyl, 4-chlorophenyl, 4-methylphenyl and 4-methoxyphenyl) immobilized on Amberlyst 15 nanostructures (nanoAmb), H<sub>2</sub>T(2 or 4-X)PP@nanoAmb are reported. The immobilization of porphyrins on the polymer was confirmed by diffuse reflectance UV-vis spectroscopy and EDX analysis. While little or no catalyst degradation was observed for a reaction time of ca. 3 h, the electron deficient porphyrins (pseudo-first order rate constants,  $k_{\text{obs}} = 0.0049\text{--}0.012\text{ min}^{-1}$ ) showed faster second order kinetics than the electron-rich ones ( $k_{\text{obs}} = 2.30 \times 10^{-5}\text{--}9.92 \times 10^{-4}\text{ min}^{-1}$ ). The order of photocatalytic activity of the porphyrins approximately correlates with the singlet oxygen quantum yield ( $\Phi_{\Delta}$ ) of the photosensitizers. Diffuse reflectance UV-vis spectra of the immobilized porphyrins demonstrated large red shift of the Soret and Q bands of the porphyrins which was more dominant in the case of H<sub>2</sub>T(4-OMe)PP. The weak overlap between the emission spectrum of the light source and the absorption spectrum of the latter was used to explain the low photocatalytic activity of H<sub>2</sub>T(4-OMe)PP@nanoAmb. The observation of a slope ( $\rho$ ) of  $-2.80$  for the oxidation of methyl phenyl sulfide and para-substituted phenyl methyl sulfides is in accord with the involvement of an electrophilic oxidation mechanism mediated by singlet oxygen species. H<sub>2</sub>TTP@nanoAmb was recovered and reused at least five times without significant loss of the catalytic activity and detectable catalyst degradation, giving a turnover number of  $5 \times 5000$  for five successive reactions. The catalyst was successfully used for large scale (up to 6.6 mmol of sulfide per batch, in a 1:10000 catalyst to sulfide molar ratio) photooxidation of a wide range of sulfides to the corresponding sulfoxide in water/acetonitrile solvent mixture.

## Introduction

Aerobic oxidation of organic compounds with the aim of conducting the oxidation reactions in the absence of toxic, high cost and usually environmentally harmful terminal oxidants is an important goal particularly from the green chemistry point of view.<sup>1–3</sup> Sulfoxides and sulfones are important intermediates in the synthesis of organic compounds, medicine and industrial applications.<sup>4–5</sup> The partial oxidation of sulfides provides sulfoxides as pharmaceutically important intermediates. Also, the oxidation of sulfides to sulfoxides is an attractive process from mechanistic standpoint.<sup>6–7</sup> However, control of product selectivity still

remains as a challenge for heterogeneous aerobic photocatalytic systems. Aerobic photooxidation of sulfides is an efficient strategy for selective oxidation of sulfides to sulfoxides.<sup>8–10</sup> On the other hand, the synthesis of novel porphyrin photosensitizers with increased photo-stability and catalytic activity has been the subject of many studies over the past decades.<sup>11–16</sup> The introduction of electron-withdrawing substituents at the periphery of the aromatic macrocycle has been generally utilized to improve the stability of porphyrins and metalloporphyrins towards oxidative decomposition under the reaction conditions. However, the formation of molecular complexes between porphyrins and different protic and Lewis acids may be used as an efficient alternative to complicated chemical syntheses. Porphyrin diacids have been the subject of many studies since the late 1960s.<sup>17</sup> However, no attention was paid to their potential for use in catalytic and photocatalytic reactions; In 2008, we have reported the first use of porphyrin diacids as catalyst for ring opening reaction of epoxide.<sup>18</sup> Recently, we have reported the improvement in the photocatalytic performance of porphyrins in the aerobic photooxidation of olefins through adduct formation with different  $\sigma$  and /or  $\pi$  acids under homogeneous and heterogeneous conditions.<sup>12–13</sup> The new metal free

<sup>a</sup> Department of Chemistry, Institute for Advanced Studies in Basic Sciences (IASBS), Zanjan 45137-66731, Iran. E-mail: zakavi@iasbs.ac.ir; szakavi@gmail.com

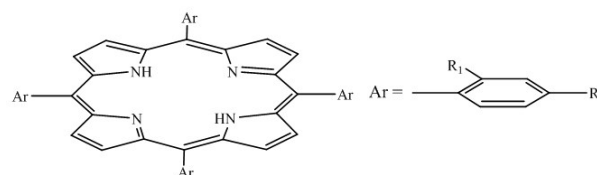
<sup>†</sup> Electronic Supplementary Information (ESI) available: [Spectral data of porphyrins, sulfides and the corresponding sulfoxides; experimental setup and general procedure of the photooxidation reactions; spectral changes upon the photooxidation of DPBF]. See DOI: 10.1039/x0xx00000x

photosensitizers are of great interest from the green chemistry point of view.<sup>19</sup> The molecular complexes and diacids were found to show higher oxidative stability, catalytic activity and significantly red shifted absorption bands, compared to those of the corresponding free base porphyrins. Furthermore, porphyrin diacids were used as efficient photosensitizers with improved oxidative stability for chemoselective aerobic photooxidation of sulfides to sulfoxides under homogeneous conditions.<sup>20</sup> However, due to highly conjugated structure of free base porphyrins and their dications, they are still sensitive to extensive degradation by singlet oxygen and other reactive oxygen species in the homogeneous phase.<sup>21</sup> Also, while using water and other polar green solvents fulfils the requirements of green chemistry<sup>22-23</sup>, most porphyrin dications and molecular complexes suffer from partial to significant dissociation into porphyrin and the acid molecules in hydrogen bond forming and coordinating solvents.<sup>13,20,24-25</sup> Interestingly, these issues may be substantially overcome by immobilization of photosensitizers on suitable organic and inorganic supports.<sup>26-27</sup> Furthermore, due to several advantages of heterogeneous catalysts over the homogeneous counterparts such as the ease of separation, increased stability and improved reusability, much attention was paid to the heterogenization of homogeneous catalysts.<sup>28-29</sup> In continuing our studies on the photocatalytic activity of porphyrins supported on Amberlyst 15 nanostructures, in the present study, a series of electron-rich and electron-deficient meso-tetra(aryl)porphyrins (Figure 1) were used for the oxidation of sulfides in water/acetonitrile mixed solvent. Furthermore, the kinetics and mechanistic aspects of the aerobic photooxidation of para-substituted methyl phenyl sulfides in the presence of the porphyrin diacids were studied. It is noteworthy that most previous kinetic studies on oxidation and photooxidation of organic compounds have been devoted to those catalyzed by non-porphyrinic photosensitizers or metalloporphyrins<sup>30-40</sup> and little attention was paid to the porphyrin photosensitizers.<sup>41-42</sup>

Previously, according to the correlations between the rate constants and Hammett substituent constants, it was shown that aerobic oxidation of sulfides with singlet oxygen is carried out through an electrophilic mechanism by initial attack of singlet oxygen on the sulfur atom.<sup>43-44</sup> Albini et al. have studied the quenching of the singlet oxygen by a series of 4-substituted thioanisoles under homogeneous conditions and provided evidence for an electrophilic mechanism for the photooxidation reaction. Moreover, a decreased reaction rate was observed in aprotic solvents. Also, the formation of persulfoxide intermediates was elucidated in these reactions.<sup>37, 45</sup>

In free base meso-tetra(aryl)porphyrins and metalloporphyrins with a planar or nearly planar porphyrin conformation, the meso substituents are almost perpendicular to the porphyrin plane and therefore there is no efficient resonance interaction between the  $\pi$  systems of the meso substituents and porphyrin core. Protonation of meso-tetra(aryl)porphyrins is accompanied with a decrease in dihedral angle between meso aryl groups and porphyrin mean plane leading to an increase in the resonance interactions between the aryl group and porphyrin  $\pi$  systems.<sup>46</sup> Accordingly, the difference between the stereoelectronic properties of the meso substituents is more pronounced in porphyrin diacids.<sup>12</sup>

It is noteworthy that highly chemoselective oxidation of sulfides to sulfoxides with turnover numbers in the range of 4500-9900 and short reaction times is achieved using the immobilized porphyrins which can be scaled up to 0.78 ml of sulfide per batch. Furthermore, little or no photocatalyst degradation was detected during the oxidation of sulfides. To our knowledge, this is the first kinetic study of the photocatalytic activity of porphyrin diacids using a series of electron-rich and electron-deficient para-substituted phenyl methyl sulfides and meso-tetra(aryl)porphyrin diacids with electron-demanding and electron-releasing meso substituents under heterogeneous conditions.



R <sub>1</sub>	R <sub>2</sub>	Porphyrin	Photosensitizer
H	H	H <sub>2</sub> TPP	H <sub>2</sub> TPP@nanoAmb
Cl	H	H <sub>2</sub> T(2-Cl)PP	H <sub>2</sub> T(2-Cl)PP@nanoAmb
CH <sub>3</sub>	H	H <sub>2</sub> T(2-Me)PP	H <sub>2</sub> T(2-Me)PP@nanoAmb
H	Cl	H <sub>2</sub> T(4-Cl)PP	H <sub>2</sub> T(4-Cl)PP@nanoAmb
H	OCH <sub>3</sub>	H <sub>2</sub> T(4-OMe)PP	H <sub>2</sub> T(4-OMe)PP@nanoAmb
H	CH <sub>3</sub>	H <sub>2</sub> T(4-Me)PP	H <sub>2</sub> T(4-Me)PP@nanoAmb

Figure 1. Photocatalysts used in this study.

## Experimental

### Instrumental

UV-vis and diffuse reflectance UV-vis (DR UV-vis) spectra were prepared on a Pharmacia Biotech Ultrospec 4000 UV-vis spectrophotometer and a Varian Cary 5000 UV-Vis-NIR absorption spectrometer, respectively. <sup>1</sup>H NMR spectra were obtained on a Bruker Avance DPX-400 MHz spectrometer. The reaction mixtures were analyzed by a Varian-3800 gas chromatograph equipped with a HP-5 capillary column and a flame-ionization detector. FT-IR spectra were prepared using a Bruker Vector 22 instrument. Nitrogen adsorption/desorption isotherms were recorded on a Belsorp Max instrument (BEL-Japan, Inc.) for porosimetry analysis. The mean diameter and size distribution of the solid catalyst before and after loading of porphyrin were measured by with a Malvern Zetasizer Nano-ZS instrument (Malvern Instruments Ltd., Worcestershire, UK) at 25 °C with a detection angle of 90°. Field-emission scanning electron microscopy (FE-SEM; Carl Zeiss ULTRA PLUS) was utilized for determination of the morphology and size of the nanoparticles. For this purpose, the crushed Amberlyst beads obtained after 5 and 24 h were placed on a clean glass slide and then vacuum-coated with gold. Digital images of the samples were taken with

HitachiS4160 field emission scanning electron microscope operating at 20 kV.

### Synthesis and immobilization of porphyrins

Meso-tetraphenylporphyrin, H<sub>2</sub>TPP and its para and ortho substituted derivatives, H<sub>2</sub>T(4-OMe)PP, H<sub>2</sub>T(4-Me)PP, H<sub>2</sub>T(4-Cl)PP, H<sub>2</sub>T(2-Me)PP and H<sub>2</sub>T(2-Cl)PP were synthesized, characterized and purified according to the literature methods.<sup>47</sup> The <sup>1</sup>H NMR, <sup>13</sup>C NMR and UV-Vis spectral data of the porphyrins are presented in ESI,† S1. Amberlyst 15 dry (Acros) was used as received. A solution of the desired porphyrin (0.08 mmol) in 25 ml ethyl acetate was added to 1.5 g Amb. The mixture was stirred for 24 h at room temperature in air and the initial pale yellow polymer turned into green. The solid was separated by centrifuging and washed with ethyl acetate until the filtrate was colorless. The amount of porphyrin loaded on the polymer was measured by UV-vis spectroscopy; Tetra-n-butylammonium hydroxide was added to the nanoAmb supported porphyrin in ethyl acetate to release the immobilized porphyrin. The released porphyrin was measured by the absorbance measurement at the wavelength of its Soret band using a calibration curve prepared by plotting the absorbance versus concentration of the respective porphyrin.

### General oxidation procedure

Unless otherwise mentioned, in all photooxidation reactions, the catalyst (0.025 mol%, 0.00066 mmol) was added to the solution of sulfide (3.3 mmol) in acetonitrile (5 mL) /water (5 mL) and stirred in a double walled cylindrical glass vessel equipped with water circulation to maintain a constant temperature (ESI,† S2). The solution was saturated with oxygen by slow purging through a glass needle for 30 min. The reactions were conducted under irradiation with a 20 W white LED lamp as the light source for the required time. Also, sunlight with an intensity of 59000 lux was used as a control reaction. The reaction progress was monitored by TLC using authentic samples. GC analysis was used to determine the yields of sulfoxide and sulfone. No sulfone product was observed in the oxidation of different sulfides in a 1:1 acetonitrile/water mixture. However, in the case of using neat acetonitrile as the solvent, sulfone product was also obtained in low yields (*vide infra*). Furthermore, as was described elsewhere,<sup>20</sup> the reaction mixture was worked up to isolate the sulfoxide product from solvent and unreacted sulfide; the catalyst was separated from the reaction mixture by centrifuge and filtration. Thin layer chromatography on a silica gel plates (with a thickness of ca. 0.25 mm and a length of 20 cm) using n-hexane and ethyl acetate in 4:1 to 10:1 volume ratios led to the separation of sulfoxide as the sole product. The <sup>1</sup>H NMR spectra of the sulfoxides summarized in the ESI,† S3) show high purity of the isolated sulfoxides. Oxidation of 1-(methylsulfinyl)benzene and other sulfides (ESI,† S3) was conducted as follows:

**1-(methylsulfinyl)benzene (1b):** Methyl(phenyl)sulfane (1a) (410 mg, 3.3 mmol) was oxidized according to the above

general oxidation procedure using H<sub>2</sub>TPP@nanoAmb (0.00066 mmol) as photocatalyst. The catalyst was filtered and separated from the reaction mixture. Crude material was separated by Thin-layer chromatography (TLC) (1:4 ratio of ethyl acetate, n-hexane) to give methyl phenyl sulfoxide (425 mg, 92%). <sup>1</sup>H NMR (400 MHz, CDCl<sub>3</sub>): δ= 7.56–7.38 (m, 5H), 2.61 (s, 3H).

### Singlet oxygen quantum yield determination

The  $\Phi_{\Delta}$  values of the photosensitizer were measured through the reaction of the reactive oxygen species with 1,3-diphenylisobenzofuran (DPBF) as a quencher of singlet oxygen and methylene blue ( $\Phi_{\Delta}$ = 0.52 in water and acetonitrile)<sup>48</sup> as a reference photosensitizer. The equation  $\Phi_{\Delta} = \Phi_{\Delta}^{std} \times (v_i \times I^{std}/U_i^{std} \times I)$  was used to determine the  $\Phi_{\Delta}$  values;  $\Phi_{\Delta}^{std}$ ,  $U_i$ ,  $U_i^{std}$ ,  $I^{std}$  and  $I$  show the  $\Phi_{\Delta}$  value of the standard photosensitizer (methylene blue, MB), the rate of DPBF ( $8 \times 10^{-4}$  M) oxidation in the presence of a given photosensitizer and a 10 W red LED lamp, the rate of DPBF oxidation in the presence of methylene blue, the number of photons absorbed by the standard solution and those absorbed by the respective photosensitizer, respectively.<sup>49</sup>

## Results and Discussion

Amberlyst beads are readily nanosized using a proper solvent. As we have reported previously<sup>11</sup>, the vigorous stirring of amberlyst and porphyrins in ethyl acetate leads to the formation of polymer supported porphyrins with a size in the range 200–240 nm. Diffuse reflectance UV-vis spectroscopy showed the immobilization of porphyrins on the acidic support in the form of porphyrin diacid (Figure 2); as seen from Figure 2 and Table 1, the immobilization of porphyrins on the polymeric support leads to the red shift of the Soret and Q(0,0) bands that is in accord with the formation of porphyrins diacids.<sup>50</sup> It is noteworthy that diprotonation of porphyrins is accompanied with the reduction of the Q bands from 4 to 2 or one bands.<sup>51</sup> For most meso-tetra(aryl)porphyrins, only one Q band, Q(0,0) is observed and the other band, Q(0,1) appears as a shoulder on the Q(0,0) band.<sup>52</sup> Furthermore, the wavelength of the Q(0,0) band of the diacids increases from H<sub>2</sub>T(2-Cl)PP to H<sub>2</sub>T(4-OMe)PP that correlates with the electron-donor ability of the meso-substituents.

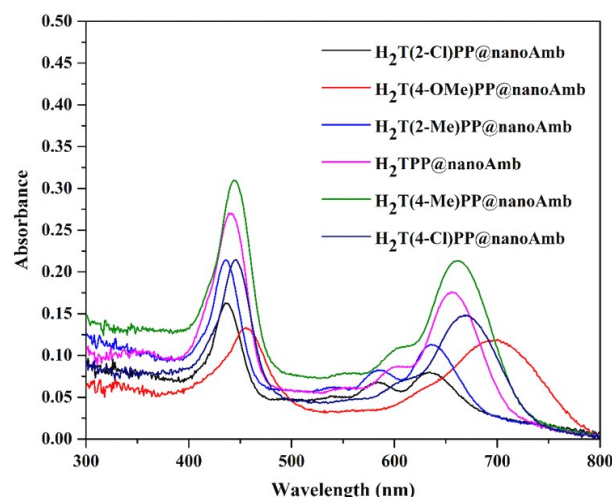


**Figure 2.** DR UV-vis spectra of H<sub>2</sub>T(2-Cl)PP@nanoAmb (black curve), H<sub>2</sub>T(4-OMe)PP@nanoAmb (red), H<sub>2</sub>T(2-Me)PP@nanoAmb (blue curve), H<sub>2</sub>TPP@nanoAmb (pink curve), H<sub>2</sub>T(4-Me)PP@nanoAmb (green curve) and H<sub>2</sub>T(4-Cl)PP@nanoAmb (dark blue).

**Table 1.** DR UV-vis spectral data of the photosensitizers.

Photosensitizer	Absorption bands ( $\lambda$ /nm)		
	Soret	Q(0,1)	Q(0,0)
H <sub>2</sub> TPP@nanoAmb	441	605	656
H <sub>2</sub> T(2-Me)PP@nanoAmb	436	587	636
H <sub>2</sub> T(2-Cl)PP@nanoAmb	435	583	634
H <sub>2</sub> T(4-Me)PP@nanoAmb	444	a	662
H <sub>2</sub> T(4-OMe)PP@nanoAmb	456	a	697
H <sub>2</sub> T(4-Cl)PP@nanoAmb	446	a	664

<sup>a</sup> The band appeared as a shoulder on the longer wavelength band.

The presence of bulky substituents at the ortho position of the phenyl groups leads to an increase in the dihedral angle between the meso aryl groups and porphyrins mean plane.<sup>46</sup> This, in turn, prevents efficient  $\pi$ - $\pi$  resonance interactions between the porphyrin core and meso substituents  $\pi$  systems and consequently a blue shift is observed in the position of the Q(0,0) band.<sup>53</sup> In contrast, the presence of strong electron-donating groups such as  $-\text{OCH}_3$  at the phenyl substituents shifts the Q(0,0) band of porphyrins to higher wavelength due to the increased electron-donation from the meso substituents to porphyrins core.<sup>46</sup> The porosimetry experiments confirmed the porous structure of the nanoparticles (Figure 3).

The nitrogen sorption isotherms of the solid catalysts shown in Figure 3 are in accord with the mesoporous structure of the catalysts and mean pore size diameters in the range of 32.4–37.8 nm, for different porphyrin@nanoAmb compounds. It is noteworthy that in NanoAmb both micropores and mesopores are found with mean pore diameters of 3.2 and 28.2 nm, respectively. As seen from Figure 3, the number of former is higher than the latter.

**Table 2.** BET analysis of nanoAmb and porphyrin@nanoAmb compounds.

Entry	Photosensitizer	$S_{\text{BET}}^a$ ( $\text{m}^2\text{g}^{-1}$ )	$V_t^b$ ( $\text{cm}^3\text{g}^{-1}$ )	Pore diameter
1	nanoAmb	85.0	0.5183	3.2, 28.2
2	H <sub>2</sub> TPP@nanoAmb	33.0	0.3000	32.4
4	H <sub>2</sub> T(2-Cl)PP@Amb	45.0	0.3600	32.6
5	H <sub>2</sub> T(2-Me)PP@nanoAmb	37.8	0.3532	37.8
3	H <sub>2</sub> T(4-OMe)PP@nanoAmb	44.2	0.3422	32.6
5	H <sub>2</sub> T(4-Me)PP@nanoAmb	46.1	0.3456	32.4
5	H <sub>2</sub> T(4-Cl)PP@nanoAmb	40.7	0.3458	32.6

<sup>a</sup>  $S_{\text{BET}}^a$  and  $V_t^b$  are the specific surface area and total pore volume, respectively.

The immobilization of porphyrins on NanoAmb is accompanied with the formation of diprotonated species of the used porphyrins. On the other hand, in the micropores, the  $\text{SO}_3\text{H}$  groups responsible for protonation of porphyrin are closer to each other and therefore the formation of a diprotonated porphyrin is more facilitated under these conditions. It should be noted that as was shown in several studies, for most porphyrins the formation of a diprotonated species is more convenient and preferred over a monoprotinated species due to thermodynamic and kinetic effects. The formation of monoprotinated is more difficult than a diprotonated one. The formation of a monoprotinated species leads to out of plane deformation of porphyrin core so that the second pyrrole ring is in a better orientation to make a strong bond with the second acid molecule. Also, the  $V_{\text{total}}$  and  $S_{\text{BET}}$  values (Table 2) show significant decrease in the BET surface area and pore volume values after the immobilization of the porphyrins. Also, DLS of the nanoparticles suspended in water showed an average diameter of 198 and 238 nm for nanoAmb and H<sub>2</sub>T(2-Cl)PP@NanoAmb, respectively (Figure 4). Accordingly, there is little or no difference between the particles size of H<sub>2</sub>T(2-Me)PP@NanoAmb and H<sub>2</sub>T(2-Cl)PP@NanoAmb. Furthermore, field-emission scanning electron microscopy (FESEM) images revealed the formation of nearly spherical nanoparticles with an average diameter of ca. 50 nm in the case of H<sub>2</sub>T(2-Cl)PP@NanoAmb.

The observed difference between the particle size obtained from DLS and FESEM is probably due to the high hydrophilicity of the used polymer.<sup>54</sup> A Particle size of ca. 50 nm was also obtained for H<sub>2</sub>TPP@NanoAmb and H<sub>2</sub>T(2-Me)PP@NanoAmb. This observation is in line with the results of BET analysis confirming the immobilization of porphyrins into the pores of the porous polymer.

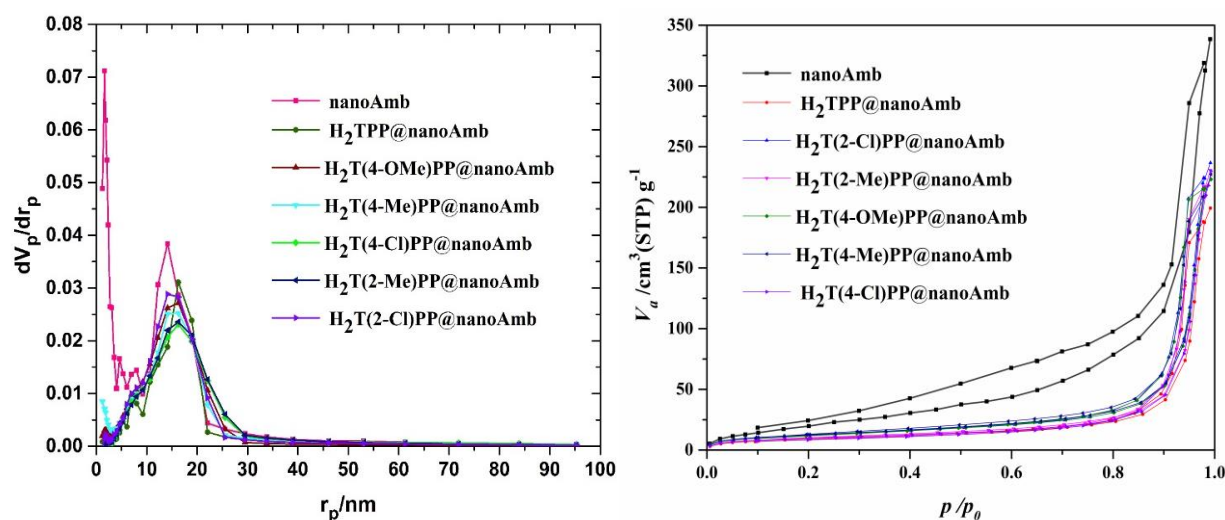


Figure 3. N<sub>2</sub> adsorption/desorption isotherms of nanoAmb and porphyrin@nanoAmb compounds.

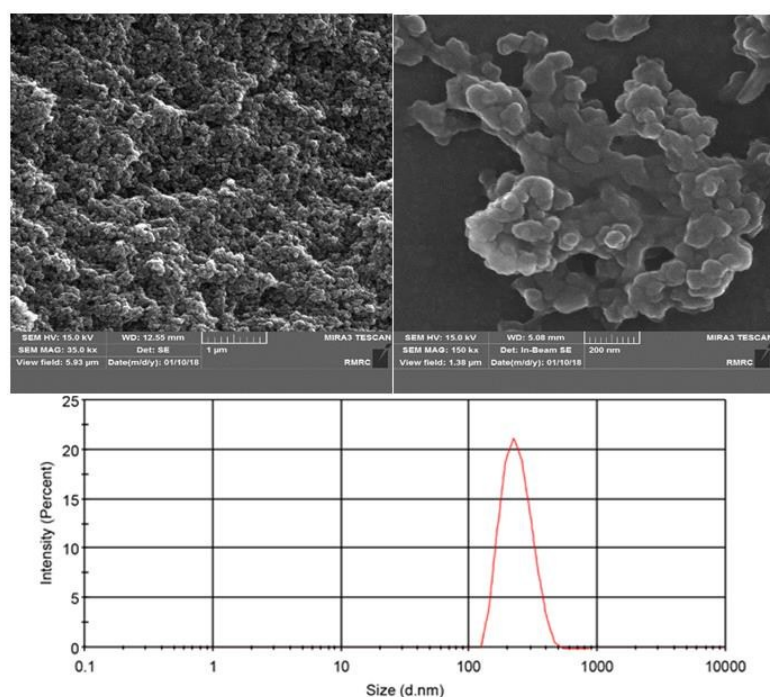
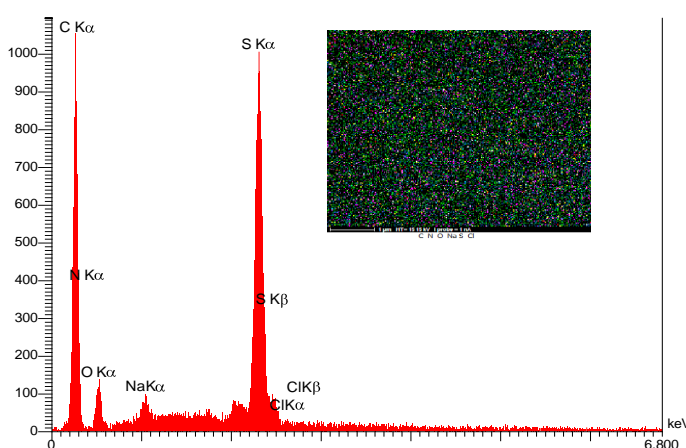


Figure 4. FE-SEM images of nanoAmb and H<sub>2</sub>T(2-Cl)PP@NanoAmb and DLS characterization of H<sub>2</sub>T(2-Cl)PP@NanoAmb.

Further evidence on the immobilization of porphyrins on nanoAmb was provided by EDX spectrum and carbon, nitrogen, oxygen, sodium and sulfur elemental mapping captured for H<sub>2</sub>T(2-Cl)PP@nanoAmb (Figure 5).

photosensitizers. Indeed, high degrees of catalyst degradation by ROS usually observed in porphyrin based catalytic systems may be prevented by increasing the substrate concentration. It should be noted that the catalyst degradation may be considered as an unwanted attack by ROS on the photosensitizer as an oxidizable organic compound. Oxidation of methyl phenyl sulfide was conducted using different catalyst to substrate molar ratios to find the optimized one (Table 3). To optimize the reaction conditions, the oxidation of methyl phenyl sulfide in the presence of H<sub>2</sub>TPP@nanoAmb was studied under various conditions (Table 3, Figure 6).

The change of solvent from neat acetonitrile to acetonitrile/water mixture (entries 1 and 2) led to a slight increase in the conversion value but a significant increase in the chemoselectivity of the reaction towards the formation of sulfoxide. Accordingly, the use of acetonitrile/water mixed solvent led to the formation of sulfoxide as nearly the exclusive product. Also, the increase in the catalyst to substrate molar ratio up to 1:5000 has little effect on the conversion value but remarkable increases in turnover number (TON) and turnover frequency (TOF) were observed (entries 2, 3 and 4). Further increase in the catalyst to substrate molar ratio increases the reaction time from 3 to 6 h for completion of the reaction (entries 5 and 6).



**Figure 5.** EDX spectrum and element map analysis of H<sub>2</sub>T(2-Cl)PP@nanoAmb. Also, the results of EDX elemental analysis of H<sub>2</sub>T(2-Cl)PP@nanoAmb are shown in the ESI,† S4.

The rate of photooxidation of sulfides and the chemoselectivity of reaction depend on different parameters including the catalyst to sulfide molar ratio, polarity of solvent, temperature, intensity and wavelength of the light source. The molar ratio of photosensitizer to substrate is among the main factors influencing the performance of porphyrin

**Table 3.** The optimized reaction conditions for the oxidation of methyl phenyl sulfide.

Entry	Catalyst:sulfide	solvent	Light Source	Time	Conversion (%) <sup>a</sup>		TON [TOF (h <sup>-1</sup> )] <sup>b,c</sup>
					Sulfoxide	Sulfone	
1	1:1000	CH <sub>3</sub> CN	White LED (20 W)	3 h	81	12	810 [270]
2	1:1000	CH <sub>3</sub> CN/H <sub>2</sub> O	White LED (20 W)	3 h	99	<1	990 [330]
3	1:3000	CH <sub>3</sub> CN/H <sub>2</sub> O	White LED (20 W)	3 h	93	<1	2790 [930]
4	1:5000	CH <sub>3</sub> CN/H <sub>2</sub> O	White LED (20 W)	3 h	92	<1	4600 [1533]
5	1:10000	CH <sub>3</sub> CN/H <sub>2</sub> O	White LED (20 W)	3 h	84	<1	8400 [2800]
6	1:10000	CH <sub>3</sub> CN/H <sub>2</sub> O	White LED (20 W)	6 h	99	<1	9900 [1650]
7	1:10000	CH <sub>3</sub> CN / H <sub>2</sub> O	White LED (20 W) (air)	8 h	90	<1	9000 [1125]
8	1:10000	CH <sub>3</sub> CN / H <sub>2</sub> O	Sunlight	6 h	92	<1	9200 [1533]

<sup>a</sup>All reactions were repeated three times, analyzed by GC and the average values were reported. The products were also characterized by <sup>1</sup>H NMR (ESI,† S1). <sup>b</sup> TON is defined as the number of product moles obtained by one mole of the catalyst. <sup>c</sup> TOF shows the turnover number of the reaction per time unit.

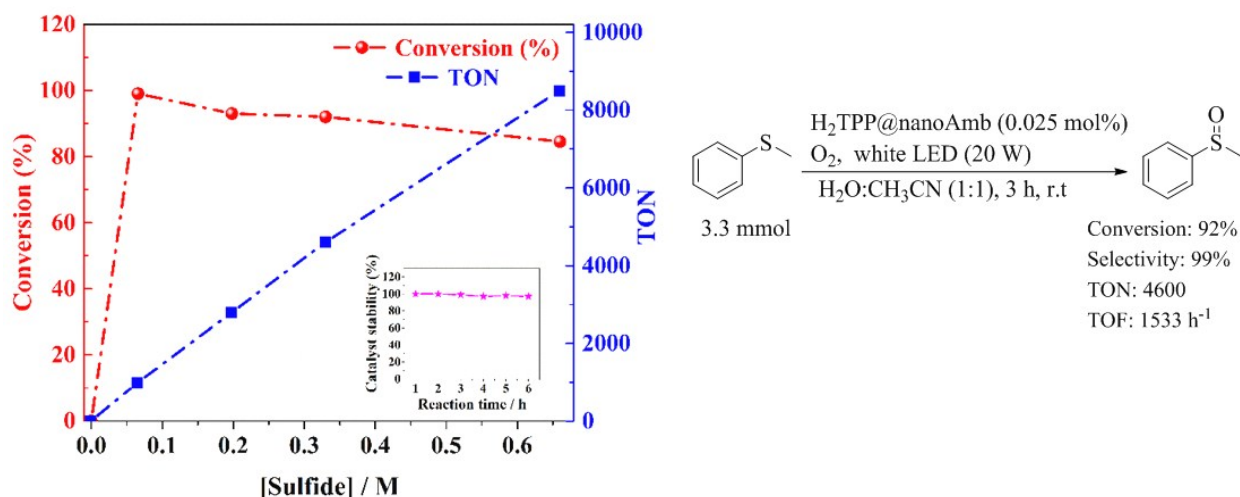


**Figure 6.** a) Photooxidation of methyl phenyl sulfide with  $\text{H}_2\text{TPP@nanoAmb}$  using 1:1000 to 1:10000 molar ratios of catalyst:substrate in acetonitrile / water under oxygen and white LED lamp (20 W); b) The optimized conditions for aerobic sulfoxidation of methyl phenyl sulfide.

**Table 4.** Effect of light source on the photooxidation of methyl phenyl sulfide catalyzed by  $\text{H}_2\text{TPP@nanoAmb}$ .<sup>a</sup>

Entry	Conversion (%)	Selectivity (%)	Photostability (%)	TON [TOF( $\text{h}^{-1}$ )]
White LED (20W)	92	100	100	4600 [1533]
Blue LED (20W)	52	100	100	2600 [866]
Red LED (20W)	21	100	100	1050 [350]
Sunlight	86	100	100	4300 [1433]

<sup>a</sup> See Table 3 for more experimental details.

The increased chemoselectivity of the oxidation reaction in the presence of water seems to be due to the stabilization of the persulfoxide intermediate by hydrogen bonds in protic solvents (*vide infra*). In other words, while the formation of hydrogen bonds stabilizes the persulfoxide intermediate, the presence of extensive hydrogen bonds around this intermediates decreases its reactivity towards the oxidation of sulfoxide. On the other hand, the use of water together with acetonitrile is consistent with the requirements of green chemistry principles. The oxidation of methyl phenyl sulfide was also studied by using air as the oxygen source (entry 7). Interestingly, a conversion value of ca. 90 % was achieved in a reaction time of 8 h that is comparable with that obtained in the presence of oxygen gas with the same pressure. It is noteworthy that little or no oxidation of methyl phenyl sulfide was observed under nitrogen gas atmosphere.

The oxidation was performed by irradiation of the reaction mixture with different light sources (Table 4) and a 20 W white LED was found to be more efficient than the corresponding blue and red LED lamps. The significantly increased conversion value in the presence of the blue lamp compared to that in the presence of the red lamp shows that the excitation at the Soret band region is mainly involved in the photocatalytic activity of  $\text{H}_2\text{TPP@nanoAmb}$ . The

emission spectra of the used LED lamps used in this study are shown in Figure 7. It is observed that the emission spectrum of the blue LED lamp overlaps more efficiently with the absorption region of the latter. In the case of the red LED lamp, the emission band appears in the range of 600 to 640 nm with maximum intensity at 615 nm.

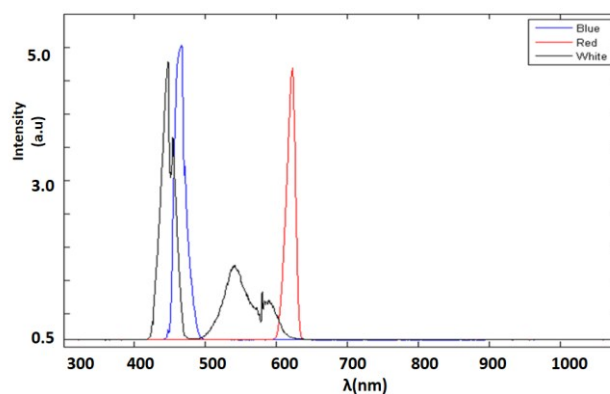


**Figure 7.** The emission spectra of the LED lamps.

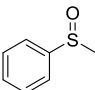
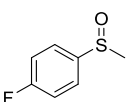
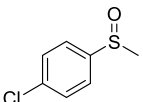
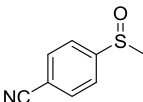
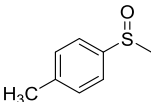
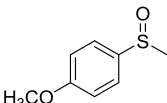
For the blue LED lamp ( $\lambda_{\text{max}} = 463 \text{ nm}$ ), a band is observed between 440–500 nm. For the white LED lamp, a narrow intense emission band ( $\lambda_{\text{max}} = 447 \text{ nm}$ ) is observed at ca. 418 to 475 nm. Also, two broad bands are observed in the range of 498 to 640 nm ( $\lambda_{\text{max}} = 547$  and 594 nm). The higher efficiency of the white LED lamp than the blue and red LED lamps seems to be due to the overlap of the latter with both the Soret and Q bands of the photosensitizer. Furthermore, a conversion value comparable with that achieved under sunlight conditions was observed. Accordingly, sunlight may be successfully used as the light source instead of the LED lamps. It is noteworthy that the oxidative degradation of porphyrin photosensitizers is a serious problem associated with the use of these compounds under oxidative conditions should be also

considered in this comparison. Interestingly, no significant catalyst degradation was observed under sunlight irradiation and the LED lamps.

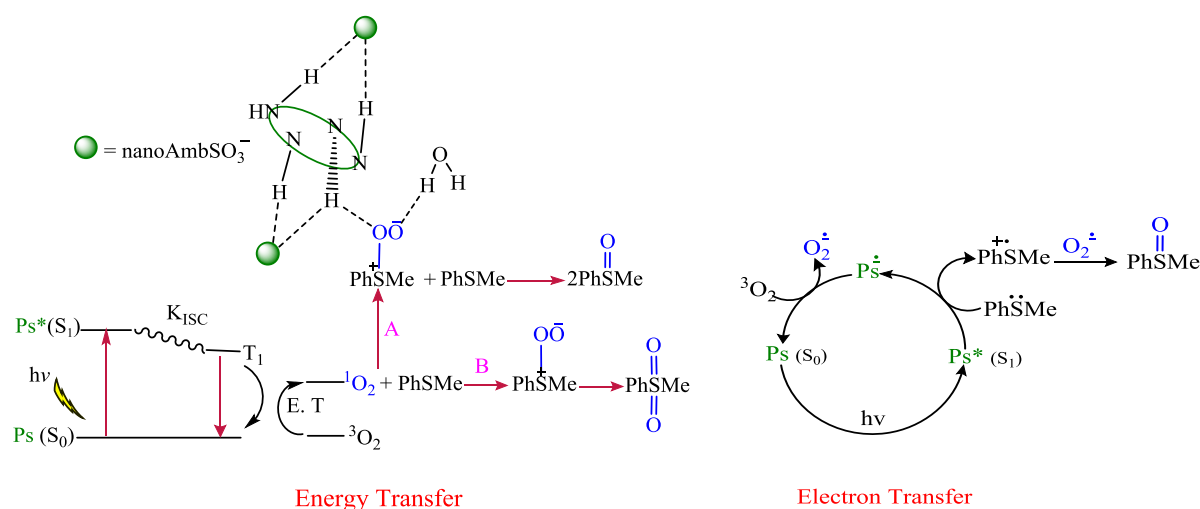
It is noteworthy that the bands around ca. 440 nm (Table 1) are appropriate for the excitation of the photosensitizers in the Soret band region. Also, the emission bands of the red LED lamp and the higher wavelength region of the white LED lamp are appropriate for the excitation at the Q band region.

In order to study the substituent effects on the reactivity of sulfides, the oxidation of various sulfides was conducted under optimized reaction conditions (Table 5). The reactions were also performed in acetonitrile.

**Table 5.** Photooxidation of different *para*-substituted phenyl methyl sulfides by  $\text{H}_2\text{TPP}@ \text{nanoAmb}$ .<sup>a</sup>

<i>Para</i> -substituent	Major product	Conversion <sup>b</sup> [Sulfoxide selectivity](%)		TON [TOF(h <sup>-1</sup> )] <sup>c,d</sup>
		$\text{CH}_3\text{CN}:\text{H}_2\text{O}$ (1:1) <sup>c</sup>	$\text{CH}_3\text{CN}^d$	
H		92 <sup>c</sup> [100]	49 <sup>d</sup> [92]	4600 <sup>c</sup> [1533]; 490 <sup>d</sup> [280]
F		99 <sup>c</sup> [100]	43 <sup>d</sup> [95]	4950 <sup>c</sup> [1650]; 430 <sup>d</sup> [246]
Cl		99 <sup>c</sup> [100]	17 <sup>d</sup> [94]	4950 <sup>c</sup> [1650]; 170 <sup>d</sup> [97]
CN		93 <sup>c</sup> [100]	3 <sup>d</sup> [75]	4650 <sup>c</sup> [1550]; 30 <sup>d</sup> [17]
$\text{CH}_3$		99 <sup>c</sup> [100]	76 <sup>d</sup> [90]	4950 <sup>c</sup> [1650]; 760 <sup>d</sup> [434]
$\text{OCH}_3$		95 <sup>c</sup> [100]	90 <sup>d</sup> [91]	4750 <sup>c</sup> [1583]; 900 <sup>d</sup> [514]

<sup>a</sup> The catalyst and substrate were used in a 1:5000 molar ratio. A 20 W white LED lamp was used as the light source. <sup>b</sup> See the footnotes of Table 3. <sup>c</sup> For a reaction time of 3 h in 1:1 acetonitrile (5 mL)/ water (5 mL) solvent mixture. <sup>d</sup> For a 1:1000 molar ratio of catalyst to substrate, using a 10 W white LED lamp as the light source and a reaction time of 105 min in neat acetonitrile. The results for the oxidation of some other sulfides are summarized in ESI,† S6.



**Scheme 1.** Proposed mechanism for the photooxidation reaction; acid catalysis with the involvement of water molecules and porphyrin dication (path A). Path B shows the formation of sulfone in the absence of acid catalysis. Ps, E.T and  $K_{ISC}$  show photosensitizer, energy transfer and intersystem crossing rate constant, respectively.

As seen from Table 5, there is little or no difference between the reactivity of *para*-substituted phenyl methyl sulfides for the reactions conducted in acetonitrile/water mixed solvent. Also, the sulfides were generally much more reactive in acetonitrile/water compared to neat acetonitrile (see also Table 3). Apparently, the hydrogen bond formation between the persulfoxide intermediate and water molecules in the former which facilitates the formation of the persulfoxide intermediates leads to a comparable reactivity for these sulfides.

**Table 6.** Temperature effect on the oxidation of methyl phenyl sulfide.<sup>a</sup>

Methyl phenyl sulfide	Temperature	
	-22 °C (2 h)	25 °C (3 h)
Sulfide	0.48	6.50
Sulfoxide	93.80	80.80
Sulfone	5.72	12.56

<sup>a</sup> Due to the relatively high freezing point of water, the reactions were conducted in acetonitrile. <sup>b</sup> A white LED lamp (20 W) was used as the light source. Catalyst and substrate were used in 1:1000 molar ratio.

The oxidation of methyl phenyl sulfide was also studied at different temperatures (Table 6) and a significant decrease in the reaction time was observed at 251 K. This observation seems to be due to the increased solubility of molecular oxygen in acetonitrile at lower temperature. Also, thermal deactivation of the triplet state of the photosensitizer by singlet oxygen at lower temperatures caused by

the increased diffusion coefficient of the  $^1O_2$  may be also involved in this observation.<sup>55</sup>

#### Kinetics of oxidation of *para*-substituted methyl phenyl sulfides

The kinetics of the photooxidation of sulfides with the singlet  $O_2$  sensitizers was studied under pseudo-first order conditions by fitting the concentration change of sulfides against the irradiation time. The plot of  $\ln(A_t/A_0)$  vs. time ( $t$ ) was linear. The slope ( $k_{obs}$ ) and the initial consumption rate of sulfides ( $v_i$ ) are determined by equations 1 and 2, respectively. Herein,  $A_t$ ,  $A_0$ ,  $k_{obs}$ ,  $t$ , and  $v$  stand for the concentration of sulfide at different time intervals ( $t$ ), the initial concentration of sulfide, pseudo-first-order rate constant, irradiation time ( $t$ ) and the consumption rate of sulfides, respectively.

$$\ln(A_t/A_0) = k_{obs} \cdot t \quad (1)$$

$$v_i = k_{obs}[\text{Sulfide}] \quad (2)$$

The oxidation of phenyl methyl sulfides with different electron-demanding and electron-donating groups at the *para* position of the phenyl group was conducted in acetonitrile (Figure 8a)

The concentration vs. time curves for the sulfides are shown in Figure 8b. An induction period of ca. 25 observed for the oxidation reactions may be due to the time required for swelling of polymer support which makes the porphyrin sites more accessible for the photooxidation reactions.

## ARTICLE

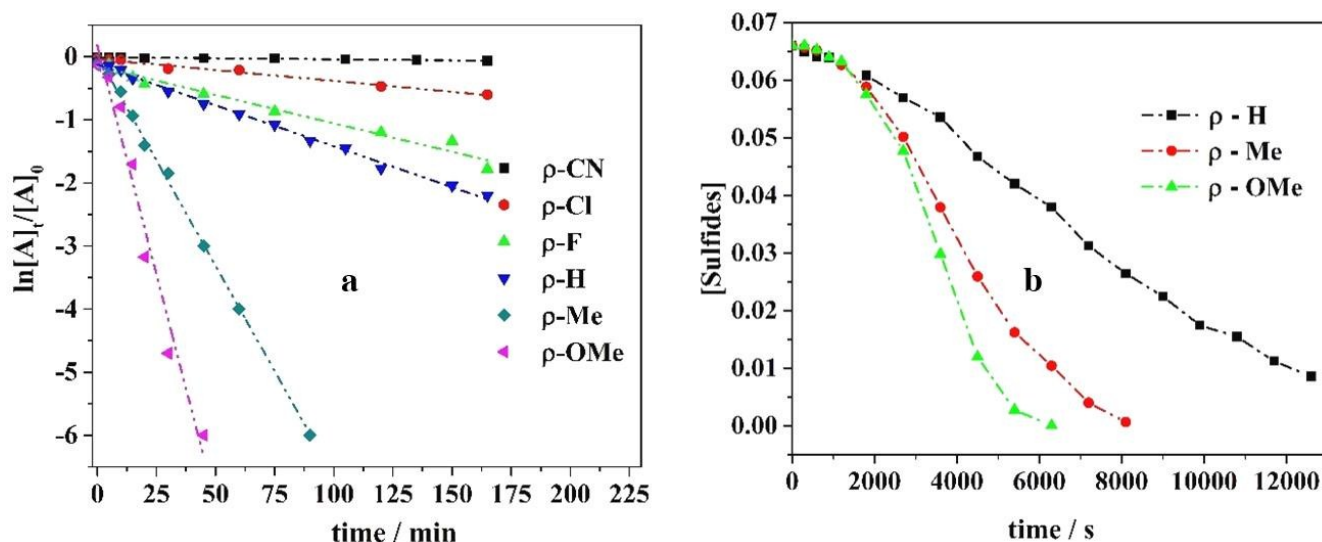


**Figure 8.** a) Kinetic curves for the photooxidation of para-substituted methyl phenyl sulfides (0.066 M) in the presence of  $H_2TPP@nanoAmb$  in acetonitrile and a 10 W white LED lamp. b) The change in the concentration of para-substituted methyl phenyl sulfides vs. time with an induction period of ca. 25 min.

**Table 7.** Oxidation of *p*-substituted-phenyl methyl sulfides in the presence of  $H_2TPP@nanoAmb$  in acetonitrile.<sup>a</sup>

<i>p</i> -X-phenyl methyl sulfide	$k_{obs}^b (\times 10^2)$ ( $\text{min}^{-1}$ )	$v_i^b (\times 10^2)$ $= k_{obs}[\text{Sulfide}]_0 (\text{M} \cdot \text{min}^{-1})$
4-Methoxyphenyl methyl sulfide	14.48	95.57
Methyl <i>p</i> -tolyl sulfide	6.68	44.09
Methyl phenyl sulfide	1.30	8.58
4-Fluorophenyl methyl sulfide	0.90	5.94
4-Chlorophenyl methyl sulfide	0.34	2.24
4-Cyanophenyl methyl sulfide	0.03	0.22

<sup>a</sup> The catalyst and substrate (0.066 M) were used in 1:1000 molar ratio. A 10 W white LED lamp was the light source. <sup>b</sup>  $k_{obs}$  and  $v_i$  show the pseudo-first order rate constants and initial consumption rate of sulfides, respectively.

The  $k_{obs}$  values, summarized in Table 7 are consistent with higher reactivity of the electron-rich sulfides so that nearly no reaction was observed in the case of methyl *para*-cyanophenyl sulfide. However, methyl *para*-methoxyphenyl sulfide and methyl *para*-tolyl sulfide are much more reactive than the other sulfides. The Hammett treatment of data for the oxidation of methyl phenyl sulfide and para-substituted phenyl methyl sulfides (Figure 9) gave a slope ( $\rho$ ) of  $-2.80$ , which is consistent with an electrophilic mechanism<sup>35</sup>. The observation of a  $\rho$  value of  $-2.8$  ( $R_2 = 0.99$ ) for the oxidation of sulfides that was comparable with that observed for the myoglobin-catalyzed sulfoxidation of the same sulfides was attributed to the involvement of an electrophilic oxidation mechanism.<sup>34, 36-37</sup> It is noteworthy that the aerobic photooxidation of organic compounds may proceed through a singlet oxygen mechanism

or a superoxide radical anion mediated charge transfer mechanism (Scheme 1). According to the previous studies, small  $\rho$  values ( $< 1$ ) and large ones ( $> 1$ ) were observed for the former and latter, respectively.<sup>37</sup> Furthermore, weak correlation between the rate constants and  $\sigma^+$  constants ( $R_2 = 0.93$ ) indicates that a single electron transfer (ET) mechanism is not considerably involved in this reaction (Figure 9) It is noteworthy that in the case of ET, referred to as the type II mechanism, the sulfide radical cation intermediate could be stabilized by resonance interactions with  $\pi$  interactions with  $\pi$  donor substituents such as  $-OCH_3$ . Also, the control reactions conducted in the presence of singlet oxygen and superoxide anion radical quenchers confirmed the presence of singlet oxygen as the main reactive oxygen species (ROS) in this catalytic system.

## ARTICLE

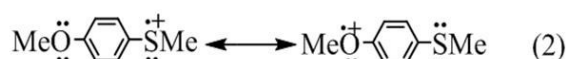
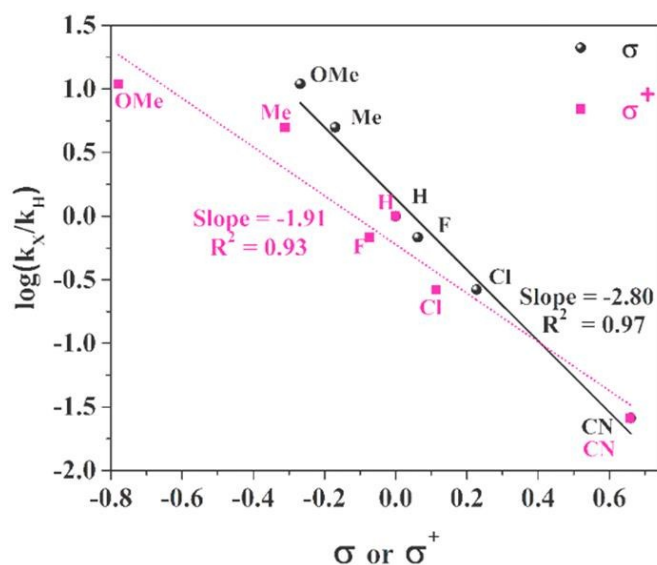


Figure 9. Linear free energy relationships for the oxidation of para-substituted methyl phenyl sulfides using  $\sigma^+$  and  $\sigma$  parameters.

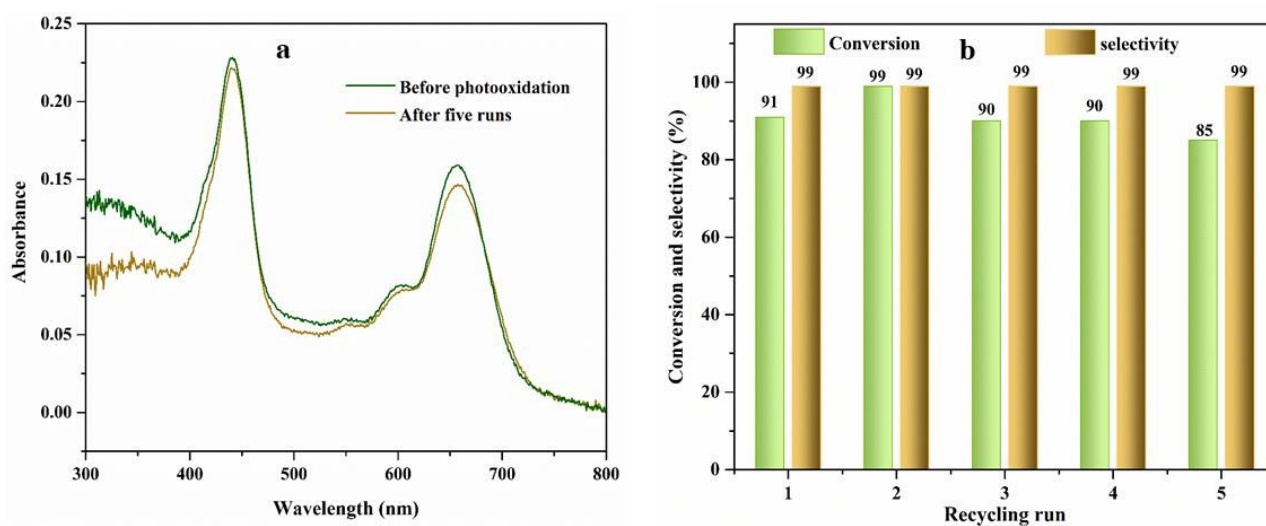


Figure 10. (a) The change in the DR UV-vis spectrum of  $\text{H}_2\text{TPP}@ \text{nanoAmb}$  separated from the reaction mixture after 5 successive runs. (b) Reusability of  $\text{H}_2\text{TPP}@ \text{nanoAmb}$  in the oxidation of methyl phenyl sulfide in water/acetonitrile solvent mixture using a 20 W white LED lamp for a reaction time of 3 h. Catalyst and substrate were used in a 1:5000 molar ratio.

## ARTICLE

The oxidation of methyl phenyl sulfide was conducted in the presence of H<sub>2</sub>TPP@nanoAmb to study the reusability of the catalyst (Figure 10b). As seen from Figure 10b, the catalysts may be recovered and reused at least five times without a significant decrease in its catalytic activity and selectivity towards the formation of sulfoxide. This observation is probably due to the significant oxidative stability of the catalyst after the 5th run.

The photocatalytic activity of different porphyrins immobilized on nanoAmb for the oxidation of methyl phenyl sulfide was studied to investigate the influence of meso substituents on the efficiency of the photosensitizers (Figure 11, Table 8).

As seen from Table 8, H<sub>2</sub>T(4-Cl)PP@nanoAmb, H<sub>2</sub>T(2-Cl)PP@nanoAmb, H<sub>2</sub>T(2-Me)PP@nanoAmb and H<sub>2</sub>TPP@nanoAmb were much more efficient photosensitizers than H<sub>2</sub>T(4-Me)PP@nanoAmb and H<sub>2</sub>T(4-OMe)PP@nanoAmb. In other words, the electron deficient porphyrins showed higher catalytic activities compared to the electron-rich ones. With respect to the negligible oxidative degradation of the porphyrins used in this study, the relative catalytic activity of the porphyrins can not be attributed to their relative oxidative stability. The higher efficiency of H<sub>2</sub>T(4-Cl)PP@nanoAmb and H<sub>2</sub>T(2-Cl)PP@nanoAmb is probably due to the heavy atom effect that facilitates the singlet to triplet intersystem crossing of the S<sub>1</sub> state of the photosensitizer; the latter is necessary for the formation of the T<sub>1</sub> state of photosensitizer responsible for the formation of singlet oxygen species.<sup>56-57</sup>

**Table 8.** Oxidation of methyl phenyl sulfide in the presence of H<sub>2</sub>T(2 or 4-X)PP@nanoAmb.<sup>a</sup>

Photosensitizer	$k_{\text{obs}} (\times 10^3)$ (min <sup>-1</sup> )	$v_i (\times 10^2)$ $= k_{\text{obs}}[\text{Sulfide}]_0$ (Mmin <sup>-1</sup> )
H <sub>2</sub> T(4-Cl)PP@nanoAmb	12.00	79.20
H <sub>2</sub> T(2-Cl)PP@nanoAmb	10.63	70.16
H <sub>2</sub> T(2-Me)PP@nanoAmb	9.09	59.99
H <sub>2</sub> TPP@nanoAmb	4.91	32.40
H <sub>2</sub> T(4-Me)PP@nanoAmb	0.99	6.53
H <sub>2</sub> T(4-OMe)PP@nanoAmb	0.02	0.13

<sup>a</sup>See the footnotes of Table 7, for more experimental details.

The extent of overlap between the emission spectrum of the light source (Figure 7) and the absorption spectrum of the porphyrinic photosensitizers (Figure 2) is a key factor determining the photocatalytic performance of the photosensitizers. The position of the absorption bands of the immobilized porphyrins (Figure 2) are summarized in Table 1. As seen from Table 1, the emission maxima of the white LED lamp less efficiently overlap with the absorption bands of H<sub>2</sub>T(4-OMe)PP@nanoAmb, due to the red shifted Soret and Q bands of this porphyrin with respect to those of the other porphyrins.

In order to elucidate the nature of reactive oxygen species (ROS) in this catalytic system, 1,3-diphenylisobenzofuran (DPBF) and 1,4-benzoquinone were used as the quencher of singlet oxygen and superoxide radical anion, respectively.<sup>58-59</sup>

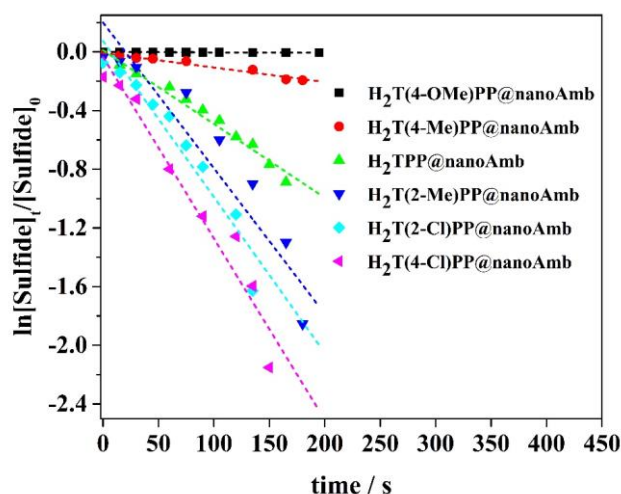
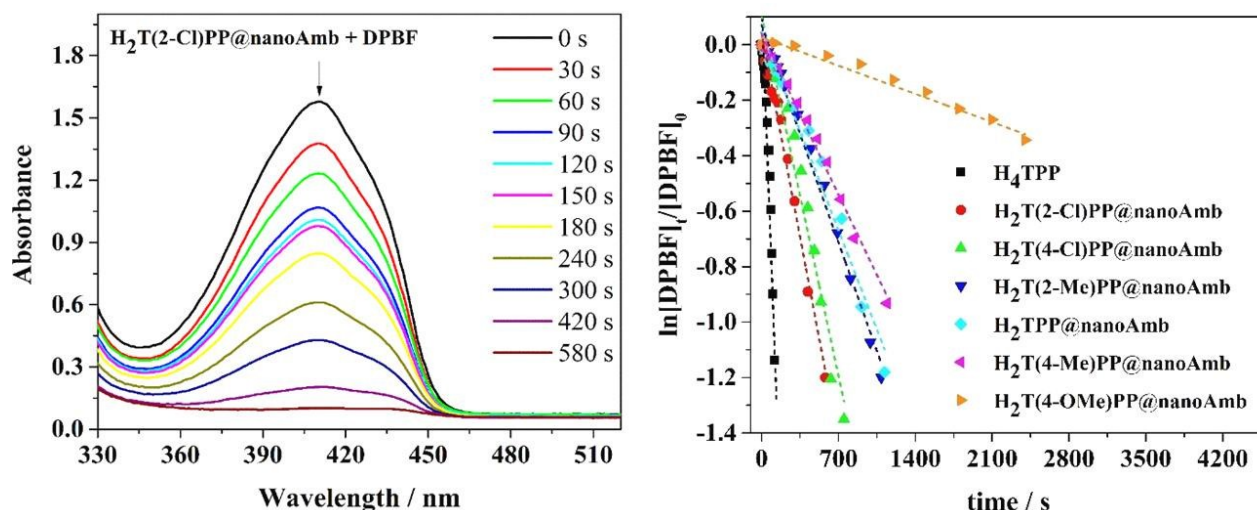


Figure 11. Kinetic curves for the oxidation of methyl phenyl sulfide in the presence of different porphyrinic photocatalysts (see the footnotes of Figure 8a for more details).

## ARTICLE



**Figure 12.** (a) The change in the UV-vis spectrum of DPBF ( $\lambda_{\text{max}} = 415 \text{ nm}$ ) in acetonitrile in the presence of  $\text{H}_2\text{T}(2\text{-Cl})\text{PP@nanoAmb}$  after irradiation with a 10 W red LED lamp (0 to 580 s); (b) Kinetic curves for the oxidation of DPBF in the presence of various photocatalysts.

As was shown in some recent studies,<sup>60–61</sup> the addition of DPBF led to nearly complete disappearance of the absorption band of DPBF at 415 nm in the UV-vis spectrum (Figure 12a) which was in accord with the presence of singlet oxygen species as the ROS (see the ESI,<sup>†</sup> S5, for the reaction conducted in the presence of the other Porphyrin@nanoAmb compounds). The kinetic curves for the oxidation of DPBF in the presence of the immobilized porphyrins (Figure 12b, Table 9) demonstrate significant influence of the peripheral substituents on the photocatalytic activity of the immobilized porphyrins. On the other hand, running the oxidation of methyl phenyl sulfide in the presence of 1,4-benzoquinone led to no detectable change in the conversion value. The latter gives evidence for the absence of superoxide radical anion in the catalytic cycle of the oxidation reaction.

The singlet oxygen quantum yield ( $\phi_\Delta$ ) of the photosensitizers measured DPBF<sup>62–63</sup> as a quencher of singlet oxygen and methylene blue as a standard are summarized in Table 9. This factor shows the efficiency of the photosensitizer in utilizing the absorbed light for the conversion of triplet oxygen to singlet oxygen species. As seen from Table 9, the exception of 4-Me, the order of photocatalytic activity of the other porphyrins correlates with the  $\phi_\Delta$  values of the photosensitizers.

**Table 9.** Kinetics data for the oxidation of DPBF and the singlet oxygen quantum yields of the photosensitizers in acetonitrile.

Porphyrin@nanoAmb	$k_{\text{obs}} (\text{M}^{-1}\text{min}^{-1})$	$10^4 v_i (\text{min}^{-1})$	$\phi_\Delta$
$\text{H}_4\text{TPP}(\text{HSO}_4)_2$	0.0107	7.00	0.203
$\text{H}_2\text{T}(2\text{-Cl})\text{PP@nanoAmb}$	0.00204	1.34	0.028
$\text{H}_2\text{T}(4\text{-Cl})\text{PP@nanoAmb}$	0.00179	1.18	0.030
$\text{H}_2\text{T}(2\text{-Me})\text{PP@nanoAmb}$	0.00109	0.71	0.016
$\text{H}_2\text{TPP@nanoAmb}$	0.000952	0.63	0.019
$\text{H}_2\text{T}(4\text{-Me})\text{PP@nanoAmb}$	0.000828	0.54	0.019
$\text{H}_2\text{T}(4\text{-OMe})\text{PP@nanoAmb}$	0.00019	0.12	0.004
MB	-	-	0.52

## Conclusion

A series of electron-rich and electron-deficient *ortho*- or *para*-substituted *meso*-tetra(phenyl)porphyrins immobilized on Amberlyst 15 nanostructures,  $\text{H}_2\text{T}(2 \text{ or } 4\text{-X})\text{PP@nanoAmb}$  were used as photosensitizers in the aerobic photooxidation of sulfides and found that: (i) the acid modified porphyrin photosensitizers showed the Soret and Q(0,0) bands in the range of 435–456 and 634–697 nm, respectively. In other words, the absorption bands of the novel photosensitizers shifted towards the therapeutic window; (ii) little or no catalyst degradation was observed for the immobilized porphyrins after a reaction time of 3 h; (iii) the electron deficient porphyrins showed much faster second order kinetics (pseudo-first order rate constants,  $k_{\text{obs}} = 0.0049\text{--}0.012 \text{ min}^{-1}$ )

than the electron-rich ones ( $k_{\text{obs}} = 2.30 \times 10^{-5}$ – $9.92 \times 10^{-4} \text{ min}^{-1}$ ); (iv) the order of photocatalytic activity of the immobilized porphyrins approximately correlated with the singlet oxygen quantum yield ( $\Phi_{\Delta}$ ) of the photosensitizers. The decreased dihedral angle between the meso substituents and porphyrin mean plane in porphyrin dications compared to that in the corresponding free base porphyrins leads to more efficient resonance interactions between the two  $\pi$  systems. This, in turn, probably leads to large difference between the photosensitizing properties of porphyrins with various aryl groups at the porphyrin periphery; (v) control reactions performed in the presence of DPBF and 1,4-benzoquinone revealed the involvement of singlet oxygen as the sole ROS; (vi) the oxidation of sulfides was scaled up to ca. 3.3 to 6.6 mmol of sulfoxide per batch, using 1:5000 and 1:10000 molar ratios of catalyst to sulfide; (vii) the catalyst was reused five times without significant loss of catalytic activity.

## Acknowledgements

Financial support of this work by the Institute for Advanced Studies in Basic Sciences (IASBS) is acknowledged. Also, the authors thank to Dr. Ehsan Ahadi Akhlaghi and Mr. Pooria Omid from the Optics Laboratory at the Department of Physics for recording the emission spectra of the LED lamps.

## References

- Z. Amara, J. F. Bellamy, R. Horvath, S. J. Miller, A. Beeby, A. Burgard, K. Rossen, M. Poliakoff and M. W. George, *Nat. Chem.*, 2015, **7**, 489–495.
- Y. Zhang, Z. Wang and X. Lang, *Catal. Sci. Technol.*, 2017, **7**, 4955–4963.
- J.-L. Shi, H. Hao, X. Li and X. Lang, *Catal. Sci. Technol.*, 2018, **8**, 3910–3917.
- Y. Xu, Z.-C. Fu, S. Cao, Y. Chen and W.-F. Fu, *Catal. Sci. Technol.*, 2017, **7**, 587–595.
- F. Bigi, A. Corradini, Ca. Quarantelli and G. Sartori, *J. Catal.* 2007, **250**, 222–230.
- M. C. Carreño, *Chem. Rev.*, 1995, **95**, 1717–1760.
- T. Nevesely, E. Svobodová, J. Chudoba, M. Sikorski and R. Cibulka, *Adv. Synth. Catal.*, 2016, **358**, 1654–1663.
- J. M. Zen, S. L. Liou, A. S. Kumar and M. S. Hsia, *Angew. Chem., Int. Ed.*, 2003, **42**, 597–599.
- Y. Xu, Z.-C. Fu, S. Cao, Y. Chen and W.-F. Fu, *Catal. Sci. Technol.*, 2017, **7**, 587–595.
- Y. Li, M. Wang and X. Jiang, *Catal. Sci. Technol.*, 2018, Accepted manuscript; DOI: 10.1039/C8CY01139G.
- A. Heydari-turkmani, S. Zakavi and N. Nikfarjam, *New J. Chem.*, 2017, **41**, 5012–5020.
- S. Zakavi, S. Hoseini and A. G. Mojarad, *New J. Chem.*, 2017, **41**, 11053–11059.
- A. G. Mojarad and S. Zakavi, *RSC Adv.*, 2016, **6**, 100931–100938.
- S. M. Ribeiro, A. C. Serra and A. d. A. R. Gonsalves, *J. Catal.*, 2008, **256** 331–337.
- L.-J. Chen, S. Chen, Y. Qin, L. Xu, G.-Q. Yin, J.-L. Zhu, F.-F. Zhu, W. Zheng, X. Li and H.-B. Yang, *J. Am. Chem. Soc.*, 2018, **140**, 5049–5052.
- G. Mele, R. Del Sole, G. Vasapollo, E. García-López, L. Palmisano and M. Schiavello, *J. Catal.*, 2003, **217**, 334–342.
- S. Aronoff, *J. Phys. Chem.*, 1958, **62**, 428–431.
- S. Zakavi, G.R. Karimipour and N. Gholami-gharab, *Catal. Commun.* 2009, **10**, 388–390.
- D. S. Su, J. Zhang, B. Frank, A. Thomas, X. Wang, J. Paraknowitsch and R. Schlögl, *ChemSusChem*, 2010, **3** 169–180.
- A. G. Mojarad and S. Zakavi, *Catal. Sci. Technol.*, 2018, **8**, 768–781.
- M. Klaper, W. Fudickar and T. Linker, *J. Am. Chem. Soc.*, 2016, **138**, 7024–7029.
- S. Y. Tang, R. A. Bourne, R. L. Smith and M. Poliakoff, *Green Chem.*, 2008, **10**, 268–269.
- C. Xing, J. Deng, R. Tan, M. Gao, P. Hao, D. Yin and D. Yin, *Catal. Sci. Technol.*, 2017, **7**, 5944–5952.
- a) S. Zakavi, M. N. Ragheb and M. Rafiee, *Inorg. Chem. Commun.*, 2012, **22**, 48–53; (b) S. Zakavi, M. N. Ragheb, *Inorg. Chem. Commun.*, 2013, **36**, 113–116.
- S. Zakavi and N. Gholami-gharab, *Polyhedron*, 2007, **26**, 2425–2432.
- N. E. Leadbeater and M. Marco, *Chem. Soc. Rev.*, 2002, **102**, 3217–3274.
- A. Heydari-turkmani and S. Zakavi, *J. Catal.*, 2018, **364**, 394–405.
- Y. Zhi, K. Li, H. Xia, M. Xue, Y. Mu and X. Liu, *J. Mater. Chem. A*, 2017, **5**, 8697–8704.
- A. G. Griesbeck, T. T. El-Idreesy and A. Bartoschek, *Adv. Synth. Catal.*, 2004, **346**, 245–251.
- R. Nasrollahi and S. Zakavi, *Eur. J. Inorg. Chem.*, 2017, 2002–2010.
- W. Nam, *Acc. Chem. Res.*, 2007, **40**, 522–531.
- D. P. Goldberg, *Acc. Chem. Res.*, 2007, **40**, 626–634.
- J. Rosenthal, B. J. Pistorio, L. L. Chng, and D. G. Nocera, *J. Org. Chem.* 2005, **70**, 5, 1885–1888.
- N. Xie, R. A. Binstead, E. Block, W. D. Chandler, D. G. Lee, T. J. Meyer and M. Thiruvazhi, *J. Org. Chem.*, 2000, **65**, 1008–1015.
- N. S. Venkataramanan, S. Prem Singh, S. Rajagopal and K. Pitchumani, *J. Org. Chem.*, 2003, **68**, 7460–7470.
- J. H. Acquaye, J. G. Muller and K. J. Takeuchi, *Inorg. Chem.*, 1993, **32**, 160–165.
- S. M. Bonesi, M. Fagnoni and A. Albini, *J. Org. Chem.*, 2004, **69**, 928–935.
- A. L. Zanolto, G. Günther S., E. Lemp M., J. R. de la Fuente and N. Pizarro U., *Photochem. Photobiol.*, 1998 **68**, 487–493.
- M. Luiz, A. T. Soltermann, A. Biasutti and N. A. Garcia, *Can. J. Chem.*, 1996, **74**, 49–54.
- R. Nasrollahi and S. Zakavi, *New J. Chem.*, 2018, **42**, 1806–1815.
- M. B. Spesia, D. Lazzeri, L. Pascual, M. Rovera and E. N. Durantini, *FEMS Immunol. Med. Microbiol.*, 2005, **44**, 289–295.
- E. Silva, M. M. Pereira, H. D. Burrows, M. Azenha, M. Sarakha and M. Bolte, *Photochem. Photobiol. Sci.*, 2004, **3**, 200–204.
- M. L. Kacher and C. S. Foote, *J. Photochem. Photobiol.*, 1979, **29**, 765–769.
- B. M. Monroe, *J. Photochem. Photobiol.*, 1979, **29**, 761–764.
- E. L. Clennan, *Acc. Chem. Res.*, 2001, **34**, 875–884.
- S. Zakavi and S. Hoseini, *RSC Adv.*, 2015, **5**, 106774–106786.
- A. D. Adler, F. R. Longo, J. D. Finarelli, J. Goldmacher, J. Assour and L. A. Korsakoff, *J. Org. Chem.*, 1967, **32**, 476–476.
- F. Wilkinson, W. P. Helman and A. B. Ross, *J. Phys. Chem. Ref. Data*, 1993, **22**, 113–262.

- 49 S.-Y. Takizawa, R. Aboshi and S. Murata, *Photochem. Photobiol. Sci.*, 2011, **10**, 895-903.
- 50 M. Meot-Ner and A. D. Adler, *J. Am. Chem. Soc.*, 1975, **97**, 5107-5111.
- 51 R. E. Haddad, S. Gazeau, J. Pécaut, J.-C. Marchon, C. J. Medforth and J. A. Shelnutt, *J. Am. Chem. Soc.*, 2003, **125**, 1253-1268.
- 52 C. J. Medforth, M. O. Senge, K. M. Smith, L. D. Sparks and J. A. Shelnutt, *J. Am. Chem. Soc.*, 1992, **114**, 9859-9869.
- 53 A. Rosa, G. Ricciardi and E. J. Baerends, *J. Phys. Chem. A*, 2006, **110**, 5180-5190.
- 54 Z. Wang, H. Liu, H. Cui, M. Zhang and Z. Zhang, *Ind. Eng. Chem. Res.*, 2015, **54**, 7219-7225.
- 55 J. Suchánek, P. Henke, J. I. Mosinger, Z. K. Zelinger and P. Kubát, *J. Phys. Chem. B*, 2014, **118**, 6167-6174.
- 56 M. Bregnhøj, M. V. Krægpøth, R. J. Sørensen, M. Westberg and P. R. Ogilby, *J. Phys. Chem. A*, 2016, **120**, 8285-8296.
- 57 W. Yang, J. Zhao, C. Sonn, D. Escudero, A. Karatay, H. G. Yaglioglu, B. I. Küçüköz, M. Hayvali, C. Li and D. Jacquemin, *J. Phys. Chem. C*, 2016, **120**, 10162-10175.
- 58 A. Casado-Sánchez, R. Gómez-Ballesteros, F. Tato, F. J. Soriano, G. Pascual-Coca, S. Cabrera and J. Alemán, *Chem. Com.*, 2016, **52**, 9137-9140.
- 59 E. A. Mayeda and A. J. Bard, *J. Am. Chem. Soc.*, 1973, **95**, 6223-6226.
- 60 J. Park, D. Feng, S. Yuan and H. C. Zhou, *Angew. Chem., Int. Ed.*, 2015, **127**, 440-445.
- 61 Z. Li, C. Liu, H. Abroshan, D. R. Kauffman and G. Li, *ACS Catal.*, 2017, **7**, 3368-3374.
- 62 P. Majumdar, X. Yuan, S. Li, , B. Le Guennic J. Ma, C. Zhang, D. Jacquemin and J. Zhao, *J. Mater. Chem. B*, 2014, **2**, 2838-2854.
- 63 K. K. Chin, C. C. Trevithick-Sutton, J. McCallum, S. Jockusch, N. J. Turro, J. Scaiano, C. S. Foote and M. A. Garcia-Garibay, *J. Am. Chem. Soc.*, 2008, **130**, 6912-6913.

View Article Online  
DOI: 10.1039/C8CY02433B

## Kinetic and mechanistic aspects of solid state, nanostructured porphyrin diacid photosensitizers in photooxidation of sulfides

Rahele Nasrollahi, Akram Heydari-turkmani, Saeed Zakavi\*

Kinetics and mechanism of aerobic photooxidation of sulfides in the presence of a series of electron-rich and electron-deficient porphyrins immobilized on Amberlyst 15 nanoparticles in the form of porphyrin diacids are reported.

